

Andreev Level Spectroscopy and Josephson Current Switching in a 3-Terminal Josephson Junction

H. Tolga Ilhan, H. Volkan Demir, and Philip F. Bagwell
 Purdue University, School of Electrical Engineering
 West Lafayette, Indiana 47907
 (November 7, 2018)

We calculate the electrical currents through a superconductor - insulator - superconductor junction which is also weakly coupled to a normal metal side probe. The voltage V applied to the normal metal terminal controls the occupation of Andreev energy levels E_n , and therefore controls the Josephson current flowing through these levels. Whenever the probe voltage crosses an Andreev level, the Josephson current changes abruptly by an amount equal to the current flowing through the Andreev level. The differential conductance along the normal metal terminal permits spectroscopy of the Andreev levels. In a short junction ($L \ll \xi_0$), the critical current switches abruptly from the Ambegaokar-Baratoff value to zero when the probe voltage is approximately equal to the superconducting energy gap ($|eV| \simeq \Delta$). The magnitude of the Josephson current switching in a long junction ($L \gg \xi_0$), and the range of probe voltages over which the Josephson current differs from its equilibrium value, are much smaller than for three-terminal ballistic superconductor - normal metal - superconductor junctions.

PACS numbers: 74.80Fp, 74.50+r, 73.20.Dx

submitted to Physical Review B-1

I. INTRODUCTION

The Andreev energy levels¹ in superconductor - normal metal - superconductor (SNS) or superconductor - insulator - superconductor (SIS) junctions, through which a large fraction of the the Josephson current flows²⁻⁹, are only weakly held in thermodynamic equilibrium with the two superconducting contacts of a Josephson junction. When the quasi-particle energy is inside the superconducting gap, quasi-particles cannot transmit into the superconductor, and also cannot be injected into the Andreev levels from the superconductor⁸. The coupled electron-like and hole-like quasi-particles which form the Andreev levels orbit in continuous periodic motion inside the normal (or insulating) region of the SNS or SIS junction. Quasi-particles in the Andreev levels are then essentially thermodynamically isolated from the superconductors, yet carry a large fraction of the supercurrent. Only inelastic scattering inside the superconductor forces the occupation factor for the Andreev energy levels towards the equilibrium Fermi occupation factor of the superconducting contacts.

An additional normal metal contact coupled to the Josephson junction can directly inject quasi-particles into the Andreev energy levels through elastic scattering processes, and therefore can directly control the occupation of the bound levels. The additional normal metal probe coupled to the Josephson junction, shown in Fig. 1, models either a scanning tunneling microscope tip or the gate electrode of a three-terminal Josephson junction¹⁰⁻¹⁶. Since the rate at which the superconducting contacts inject quasi-particles into the Andreev levels through in-

elastic processes is extremely small, even a normal metal probe only weakly in contact with the Josephson junction will inject quasi-particles into the Andreev levels much faster than the superconducting electrodes. As long as the normal metal probe is only weakly in contact with the Josephson junction through a tunnel barrier, the main effect of the probe is therefore to fix the occupation factor of the Andreev levels, leaving the wavefunctions of the Andreev levels essentially unchanged from the isolated Josephson junction.^{8,12,13} The normal metal probe therefore forces the effective Fermi level of the bound Andreev states towards the Fermi level of the probe, rather than the Fermi level of the superconductors.

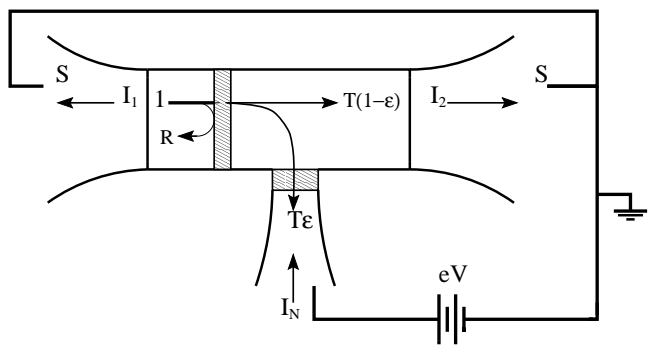


FIG. 1. Josephson junction coupled to a normal metal side probe. The probe is biased at a voltage V with respect to the two superconductors. This normal metal probe controls the occupation factor of the bound Andreev levels, since quasi-particles having energies inside the superconducting gap cannot transmit into either superconductor.

Controlling the Andreev bound state occupation

through a normal terminal leads both to an abrupt switching of the Josephson current $I(V)$, and a peak in the differential conductance $dI_N(V)/dV$ along the normal terminal, whenever the probe voltage V is equal to the energy of an Andreev level.¹² As a bound level is populated or depopulated by the probe voltage, the Josephson current changes by an amount equal to the current carried by the bound level. As the Andreev level is being filled by the probe, the differential conductance dI_N/dV along the normal metal lead also has a peak. The density of Andreev levels in the SNS junction can therefore be detected by measuring the differential conductance dI_N/dV along the normal metal lead. Together with a phase - biasing network of large area Josephson junctions, this differential conductance spectroscopy can be used to directly map¹⁷ the energy - phase relation $E_n(\phi)$ and current - phase relation $I_n(\phi)$ of the Andreev energy levels in different types of Josephson junctions.

One can obtain a more quantitative understanding of the Josephson current switching and Andreev level spectroscopy in any Josephson junction in the limit where the normal metal probe is weakly coupled to the junction. The total Josephson current $I(\phi, V)$ is a sum of the currents flowing through discrete energies inside the superconducting energy gap I_d and through the continuum of energy levels outside the gap I_c as $I(\phi, V) = I_d(\phi, V) + I_c(\phi)$. Here $\phi = \phi_2 - \phi_1$ is the superconducting phase difference. The contribution I_c to the Josephson current by scattering states outside the superconducting energy gap is essentially unchanged by the probe voltage V , since the superconducting contacts can easily inject quasi-particles into Andreev resonances in the energy continuum. Scattering states outside the energy gap therefore remain in equilibrium with the superconducting contacts. The portion of the Josephson current I_d flowing through the Andreev levels, however, is¹²

$$I_d(\phi, V) = \sum_n \{ I_n^-(\phi) f(E_n^-(\phi) - eV) + I_n^+(\phi) f(E_n^+(\phi) - eV) \} . \quad (1)$$

In Eq. (1) the $I_n^\pm(\phi) = (2e/\hbar)(dE_n^\pm(\phi)/d\phi)$ are the currents carried by ‘forward’ and ‘reverse’ Andreev levels E_n^\pm before adding the side probe. The probe voltage eV appears inside the Fermi factors f in Eq. (1) as an effective electrochemical potential for the Andreev levels. Therefore, Eq. (1) implies that the contribution of each Andreev level to the total Josephson current can be switched on or off by varying the probe voltage V .

The tunneling current through the normal metal probe measures the local density of quasi-particle states in the Josephson junction. It is well known from tunneling spectroscopy of normal metals that the tunneling current is proportional to the local density of states at the surface¹⁸, and this also holds true for superconducting tunnel junctions. The tunneling spectroscopy of Andreev levels in a Josephson junction, using tunneling current from the normal probe then, corresponds to

$$\frac{dI_N}{dV} = \frac{4e^2}{h} \sum_{n,\alpha} \left(\frac{\Gamma_n^2}{\Gamma_n^2 + (eV - E_n^\alpha)^2} \right) , \quad (2)$$

when $|eV| < \Delta$. Here Γ_n is the width of Andreev level n , which is proportional to the coupling constant ϵ . Although Ref.¹² derived Eqs. (1)-(2) only for a ballistic SNS junction, they should describe any type of Josephson junction. The numerical simulations we present in the following sections follow from the scattering theory in Appendix A, and can be understood using Eqs. (1)-(2).

In this paper we consider the Josephson current switching $I(V)$ and differential conductance spectroscopy of the Andreev levels $dI_N(V)/dV$ as we vary the voltage V along the normal terminal in a three-terminal SIS junction. The details of the Josephson current switching and spectroscopy of the Andreev states in a three-terminal SIS junction differ considerably from the ballistic SNS junction¹². In a short SIS junction, having $(L \ll \xi_0)$, the presence of an insulator forces the Andreev energy levels to the edge of the superconducting energy gap. The Josephson current in a short SIS junction therefore switches to zero when the voltage on the normal terminal is approximately equal to the energy gap, i.e. $eV \simeq \Delta$, as we discuss in section 3. Section 4 shows that the terminal I-V characteristics of SIS Josephson junctions longer than the healing length ($L \gg \xi_0$) are more complex than those of short SIS junctions. The size of the nonequilibrium Josephson current, the regularity of its switching behavior, and the voltage range over which the terminal currents are constant, are sensitive both to the barrier transmission T and the position of the tunnel barrier in the junction. We also discuss the special limiting case where the long SIS junction has inversion symmetry²⁷.

II. SHORT JOSEPHSON JUNCTION

In a short SNS junction ($L \ll \xi_0$), the Josephson current flowing into either superconductor switches on or off as we vary the bias voltage on the side probe. It is well known both that short Josephson junctions contain only two Andreev levels, and that all the Josephson current flows through these levels ($I_c = 0$). Depopulating (or populating) both levels therefore forces the Josephson current to zero. Consider the SIS junction having transmission probability $T = 2.5\%$ in Fig. 2. The two Andreev levels $E_n(\phi)$ for the SIS junction are shown in Fig. 2(a). The horizontal lines in Fig. 2(a) correspond to bias voltages near the energy gap, namely $eV = \pm 0.995\Delta$. For positive bias voltages, injection of a quasi-particle from the normal metal terminal fills any Andreev level having energy less than $E_n \leq eV$. When only the lowest Andreev level satisfies $E_n \leq eV$, only the lowest energy level contains a quasi-particle. Consequently, when $eV \leq \sqrt{R}\Delta$,⁹ the Josephson current through the SIS junction is nearly the same as without the probe, i.e. we

recover the standard Ambegaokar-Baratoff result^{9,19-25}, as shown in Fig. 2(b).

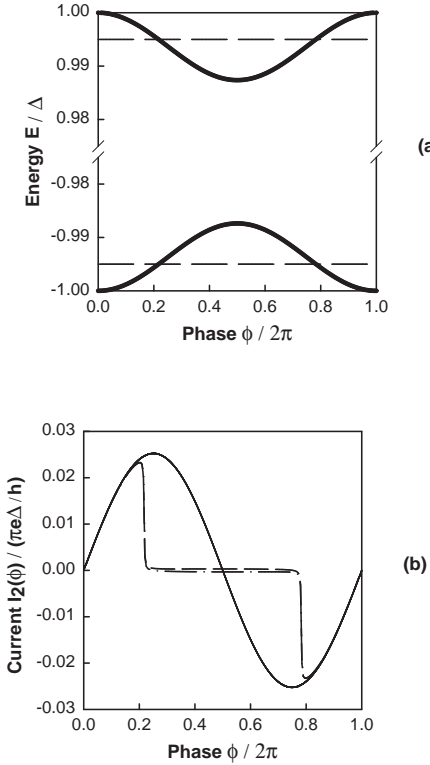


FIG. 2. (a) Andreev levels $E^\pm(\phi)$ (solid) and bias voltage $eV = \pm 0.995\Delta$ (dashed) in a short SIS junction. (b) The probe voltage crossing an Andreev level forces the Josephson current to zero, except for a small leakage current.

By varying the gate voltage, we can switch the Josephson current in a short SNS junction on or off. At a fixed phase difference, the two Andreev levels carry equal amounts of current but in opposite directions. Therefore, when both Andreev levels are filled (or empty) the Josephson current is nearly zero as shown in Fig. 2(b). We also conclude that the Josephson current-phase relation is nearly the same whether the side probe has a negative or positive bias voltage. The small difference between the two Josephson currents for $eV = \pm 0.995\Delta$ shown in Fig. 2(b) is due to the small leakage current from the gate. The leakage current is small because the coupling strength $\epsilon = 0.1\%$ in Fig. 2. The small leakage current implies that, as we vary the gate voltage between $\sqrt{R}\Delta \leq eV \leq \Delta$, the Josephson current switches from the Ambegaokar-Baratoff value to approximately zero.

Reducing the insulator transmission T forces the switching voltage and differential conductance peak towards the energy gap, i.e. $eV = \Delta$, as shown in Fig. 3. In Fig. 3 the transmission probability decreases from $T = 100\%$, 36% , 12% , the probe coupling is weak ($\epsilon = 0.1\%$ in (a)-(b) and $\epsilon = 5\%$ in (c)), and we fix

$\phi = 0.3(2\pi)$ (b)-(c). With decreasing transmission T , an energy gap opens and forces the Andreev levels to the superconducting gap edge in Fig. 3(a). Lowering the transmission coefficient in SIS junctions, therefore forces the switching voltage and differential conductance peak towards the superconducting gap at $eV = \Delta$, as shown in Fig. 3(b)-(c), respectively.

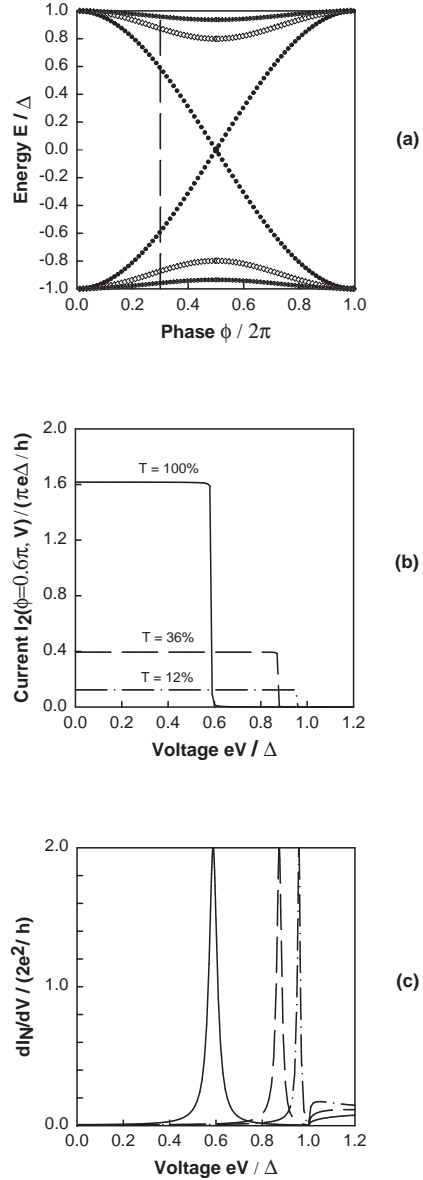


FIG. 3. (a) Andreev levels $E^\pm(\phi)$, (b) Josephson current $I(\phi, V)$, and (c) differential conductance $dI_N/dV(\phi, V)$ along the normal metal probe. Decreasing transmission probability ($T = 100\%$, 36% , 12%) forces both the switching voltage in (b) and peak in the differential conductance in (c) towards the gap edge.

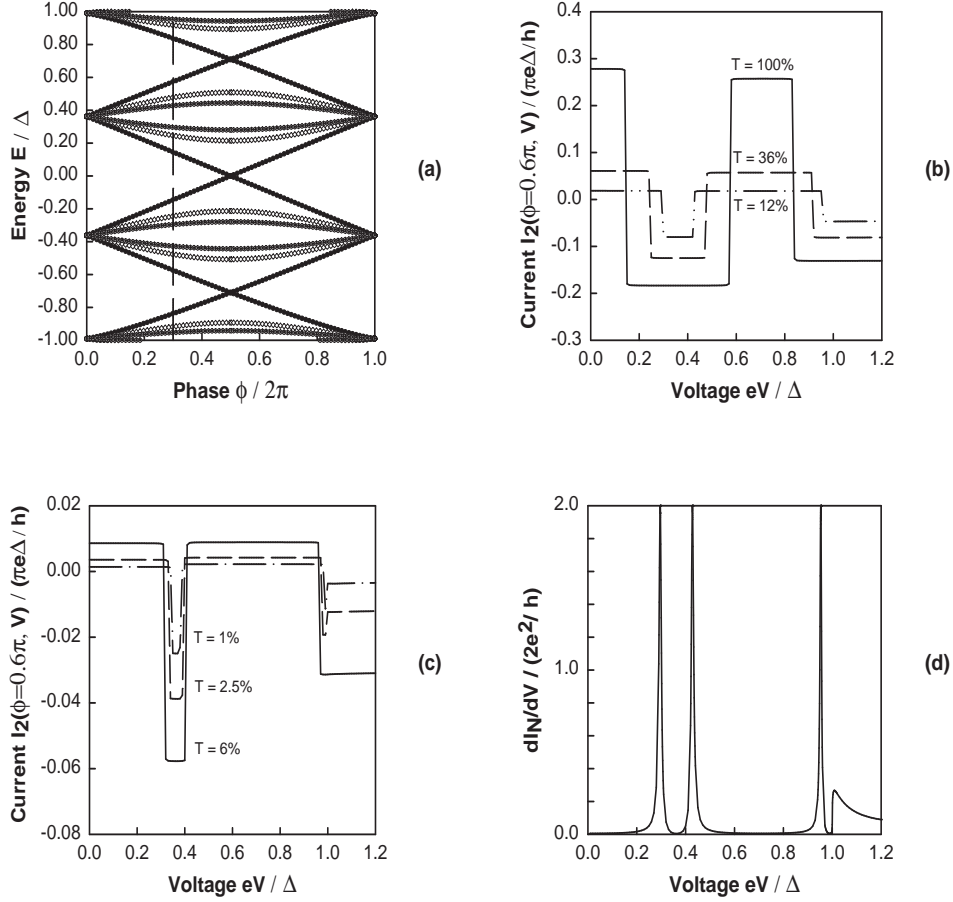


FIG. 4. A long ($L > \xi_0$) SIS junction which has inversion symmetry. (a) Andreev levels, (b)-(c) Josephson currents, and (d) differential conductance along the normal probe. With decreasing barrier transmission, the nonequilibrium Josephson current exceeds the equilibrium current ($V = 0$) over a narrow voltage range. Ballistic junctions ($T = 100\%$) have the largest currents both in and out of equilibrium.

We can understand why the Josephson current in Fig. 3(b) is constant before switching off when the bias voltage crosses an Andreev level at $E_n = eV$ by considering the Andreev level structure in Fig. 3(a). For a positive bias voltages and fixed phase difference ϕ , the lowest Andreev level ($E_n \leq 0$) carries the total current until the upper level crosses $E_n = eV$. The zero temperature Josephson current is therefore unchanged for voltages smaller than $|eV| \leq |E_n|$. Decreasing T reduces the Josephson current in Fig. 3(b), since the lowest Andreev level carries a smaller current with smaller transmission T . The differential conductance dI_N/dV along the probe also has a peak whenever the bias voltage crosses a new Andreev level, as shown by comparing Fig. 3(b)-(c).

III. LONG JOSEPHSON JUNCTION

Spectroscopy of the Andreev levels and the Josephson current switching as a function of the gate voltage V change significantly when the junction length L becomes comparable to the BCS healing length ξ_0 . The number of levels is proportional to L/ξ_0 , so more Andreev levels $E_n(\phi)$ become bound in the pair potential well. In addition, the interference pattern between quasi-particle waves multiply reflected between the NS interface and the tunnel barrier depends on the junction length L/ξ_0 and the symmetry of the SIS junction²⁷. The current $I_n(\phi)$ flowing through the Andreev levels also depends on the junction length and symmetry of the scattering potential. To illustrate the variation of the Josephson current and probe current with these parameters, we study in this section a ‘symmetric’ SIS junction (where the impurity is in the middle of the normal metal region) and an ‘asymmetric’ junction lacking this inversion symmetry.

A. Symmetric Junction

It has long been known that the net equilibrium Josephson current in long SNS and SIS junctions is a small difference between much larger positive and negative currents flowing in equilibrium^{3,4,26,7-9}. For a Josephson junction in equilibrium, adding these large counterflowing currents produces a net current proportional to the barrier transmission T . Ref.²⁷ quantified the magnitude of the larger electrical currents (which cancel in equilibrium). In long, low transmission Josephson junction having inversion symmetry Ref.²⁷ showed that these larger currents are proportional to \sqrt{T} . Ref.²⁷ also suggested that one could probe these ‘giant’ currents by inducing a non-equilibrium population of the Andreev levels.

Fig. 4 shows the (a) Andreev levels, (b)-(c) Josephson currents, and (d) differential conductance along the normal probe in a long ($L = 6.6\xi_0$), symmetric SIS junction. The probe coupling in Fig. 4 is also weak, so that $\epsilon = 0.1\%$ in (a)-(c) and $\epsilon = 5\%$ in (d). The Andreev levels in Fig. 4(a) do not split at $\phi = 0, 2\pi$, as the transmission decreases from $T = 100\%$ (filled) to 36% (empty) or 12% (dotted), as one might expect.⁹ The Andreev levels in the symmetrical junction do not split at $\phi = 0, 2\pi$ because of a geometrical symmetry in the junction. Upon normal reflection from the tunnel barrier, a quasi-particle cannot tell whether it is on the left or right side of the barrier when $\phi = 0, 2\pi$. Therefore, the energy levels at $\phi = 0, 2\pi$ are unaffected by the presence of a tunnel barrier. When the phase difference is not $\phi = 0, 2\pi$ this geometrical symmetry is broken, so the degenerate energy levels do split at any phase value other than $\phi = 0, 2\pi$. This failure of the energy levels to split at $\phi = 0, 2\pi$ in s-wave SIS junctions is exactly the same geometrical symmetry leading to the ‘midgap’ energy levels in Josephson junctions formed from d-wave superconductors^{28,29}.

To obtain a formula for the Andreev levels in Fig. 4(a), we set $a = L/2$ in Eqs. (7)-(8) of Ref.⁹. The ‘effective phase’ α in the symmetric SIS junction then simplifies to

$$\sin(\alpha) \simeq \alpha \simeq 2\sqrt{T}|\sin(\frac{\phi}{2})|, \quad (3)$$

leading to the Andreev levels

$$E_n^\pm \simeq \frac{\Delta\xi_0}{L + 2\xi_0}(2\pi n - \pi \mp 2\sqrt{T}|\sin(\frac{\phi}{2})|). \quad (4)$$

The geometrical symmetry also produces an additional resonant enhancement of the Josephson current in each Andreev level. By setting $a = L/2$ in Eqs. (7), (15), and (16) of Ref.⁹, we obtain

$$I_n^\pm = \pm \frac{ev_F}{L + 2\xi(E_n^\pm(\phi))} \sqrt{T} \cos(\frac{\phi}{2}). \quad (5)$$

for symmetrical junction. In short junctions the variation of $E_n^\pm(\phi)$ in Eq. (5) produces an Andreev level current proportional to T^9 , while in long junctions $E_n^\pm(\phi) \simeq$

constant when the barrier transmission $T \ll 1$. Consequently, $I_n \propto \sqrt{T}$ in long, low transmission, symmetric Josephson junctions, again for the same reasons as the resonant enhancement of Josephson current in d -wave superconducting junctions.²⁹ Eqs. (4)-(5) are the same as found by Wendum and Shumeiko in Ref.²⁷.

Fig. 4(b)-(c) shows the Josephson current switching for the long, low transmission, symmetric Josephson junction. (We fix $\phi = 0.3(2\pi)$ in Fig. 4(b)-(d).) The changes in the Josephson current have equal magnitudes until the gate voltage approaches the energy gap, similar to the ballistic SNS junction¹². Unfortunately, this switching occurs only over a much narrower range of gate voltages than in the ballistic SNS junction. Comparing Figs. 4(b)-(c) we see that the range of gate voltages where the Josephson current changes from its equilibrium value becomes much narrower as the transmission decreases. The \sqrt{T} versus T effect is also clearly visible in Fig. 4(c), though none of the ‘giant’ Josephson currents²⁷ in Fig. 4(c) are as large as the ballistic SNS junction in Fig. 4(b). The ballistic SNS junction has both the largest equilibrium Josephson current and the largest switching amplitude of the Josephson current with variation in the gate voltage.

The range of voltages over which the Josephson current differs from its equilibrium value in a ballistic SNS junction is approximately half of the energy gap, as shown in Fig. 4(c). In contrast, the Josephson current in a long SIS junction with inversion symmetry differs from its equilibrium value only over a very narrow range of voltages, as also shown in Fig. 4(c). We can infer from Eq. (4) that the range of voltage over which the ‘giant’ Josephson current of Ref.²⁷ occurs is proportional to $\sqrt{T}\Delta(\xi_0/(L + 2\xi_0))$, namely the bandwidth of the Andreev level. Fig. 4(d), for the same junction having transmission probability $T = 12\%$, shows the differential conductance dI_N/dV along the probe has a peak whenever the probe voltage crosses a new Andreev level.

B. Asymmetric Junction

Fig. 5 shows the (a) Andreev levels, (b)-(c) Josephson currents, and (d) gate current in an asymmetric junction where $a = L/5$. The Andreev levels in Fig. 5(a) correspond to a long SIS junction ($L = 6.6\xi_0$) where the transmission probability $T = 100\%, 36\%, 12\%$ and the coupling strength $\epsilon = 0.1\%$. The presence of an impurity removes all of the degeneracy in the Andreev level spectrum in an asymmetric SIS junction, though some energy levels split more than others. For example, the energy gap at $\phi = \pi$ and $|E| \simeq 0.7\Delta$ is much smaller than the other gaps.

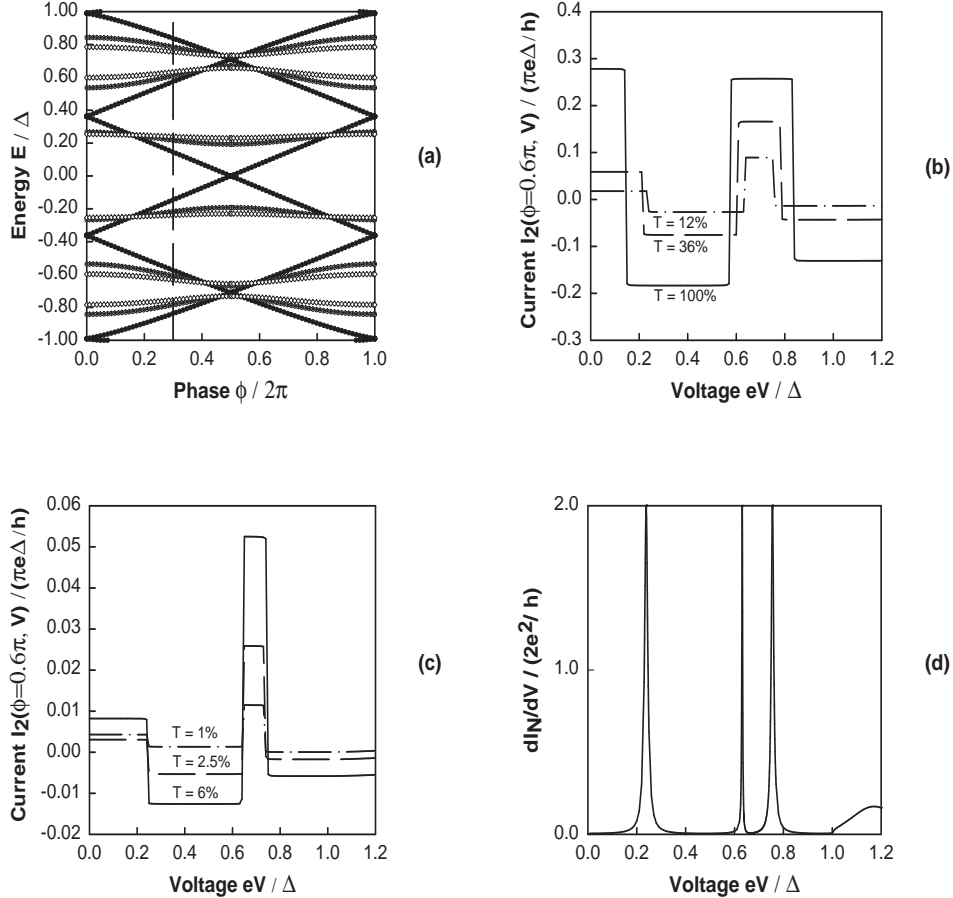


FIG. 5. A long ($L > \xi_0$) SIS junction without inversion symmetry. (a) Andreev levels, (b)-(c) Josephson currents, and (d) differential conductance along the normal probe. A small Andreev energy gap leads to large nonequilibrium Josephson currents, but over a narrow voltage range. Larger Andreev energy gaps produce a nonequilibrium current of nearly the same magnitude as the equilibrium current, but over a wider voltage range. Ballistic junctions ($T = 100\%$) again have the largest currents, both in and out of equilibrium.

The small energy gaps present in the Andreev level spectrum, even in asymmetric SIS junctions, produce Andreev level currents which approach the ‘giant’ \sqrt{T} variation of the Josephson current of Ref.²⁷. Figs. 5(b)-(c) show the Josephson current switching in a long SIS junction ($L = 6.6\xi_0$) having coupling strength $\epsilon = 0.1\%$. We also fix the phase at $\phi = 0.3(2\pi)$ in Figs. 5(b)-(d). For the small transmission coefficients in Fig. 5(c), we see that the equilibrium Josephson current decreases much more rapidly than the current carried in the Andreev levels near $|E| \simeq 0.7\Delta$ (due to the small energy gap near $|E| \simeq 0.7\Delta$). Comparing the asymmetric junction of Fig. 5(c) and the symmetric junction of Fig. 4(c) shows that the magnitude of the current switching due to occupation of a new Andreev level can be nearly the same for both symmetrical and asymmetrical junctions. Therefore, inversion symmetry is not a necessary condition for an Andreev level to carry a ‘giant’ Josephson current.

The ballistic junction ($T = 1$) again carries the largest equilibrium and nonequilibrium Josephson current.

One further difference between the long SIS junctions with inversion symmetry and the asymmetric junctions is that the Josephson current switches by different amounts in the asymmetric junctions when $eV < \Delta$, as shown in Fig. 5(b)-(c). In an asymmetric junction, magnitude of the current $|I_n|$ flowing through each Andreev level is in general different, while for symmetric junctions they are nearly the same (as long as $|E_n|$ is not too near the gap edge). Fig. 5(b)-(c) and Fig. 4(b)-(c) also show that Josephson current does not fall exactly to zero when probe voltage exceeds the energy gap ($eV \geq \Delta$). As emphasized in Ref.¹², this is because the leaky Andreev levels outside the superconducting gap carry a portion of the Josephson current. The normal metal probe therefore provides a means of doing energy spectroscopy of the Josephson current, making it possible to measure this

‘continuum’ contribution to the current. Spectroscopy of the bound levels is again shown by the differential conductance dI_N/dV in Fig. 5(d) for transmission $T = 12\%$.

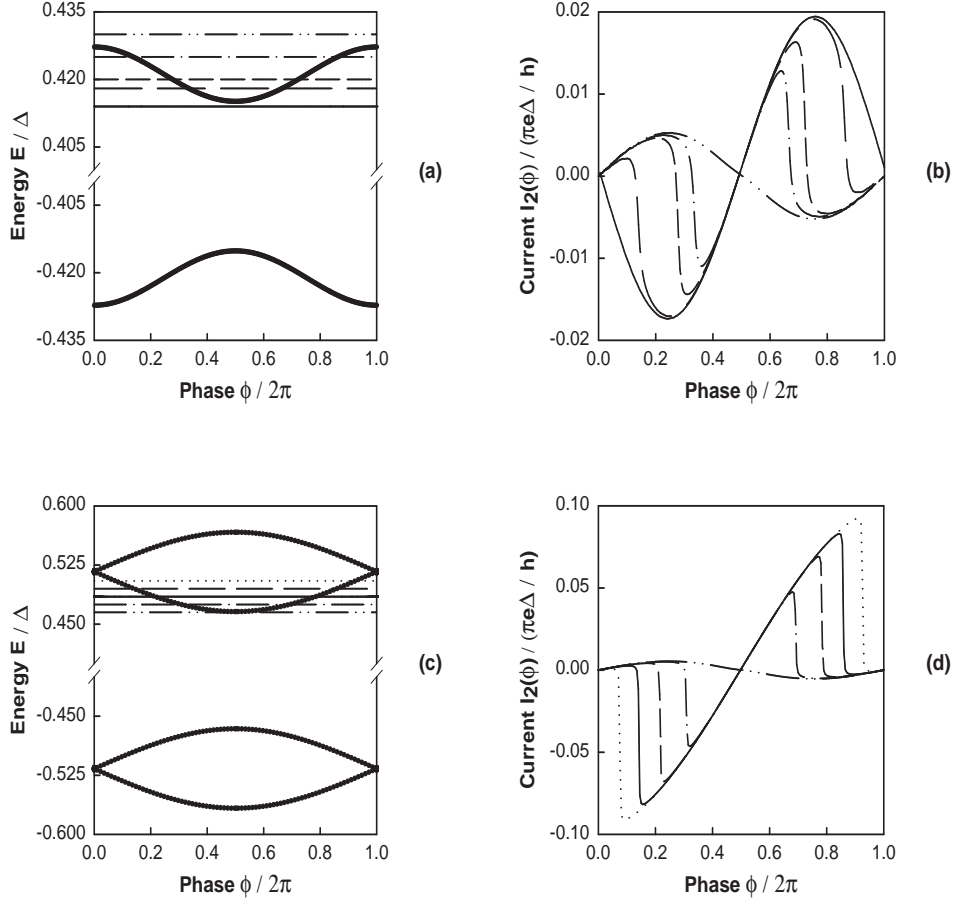


FIG. 6. Andreev levels $E^\pm(\phi)$ and nonequilibrium Josephson current-phase relation $I(\phi, V)$ for a junction without inversion symmetry (a)-(b) and with inversion symmetry (c)-(d). The current phase relations are similar, except for the larger current magnitude in the symmetric junction.

C. Current-Phase Relation

The current flow through bound Andreev levels can also be observed in the current-phase relation of a Josephson junction.¹⁷ In Fig. 6, we show the Andreev levels and current-phase relation in a long ($L = 4\xi_0$) SIS junctions. The asymmetric junction in (a) and (b) has the impurity placed one third of the distance across the normal region ($a = L/3$), while the symmetric junction in (c) and (d) has $a = L/2$. For both junctions, the transmission probability $T = 2.5\%$ and the coupling strength $\epsilon = 0.1\%$. We apply gate voltages to the SIS junction which intersects an Andreev level, namely $eV = \pm 0.414, 0.418, 0.420, 0.425, 0.430\Delta$ in (a) and $eV = \pm 0.465, 0.475, 0.485, 0.495, 0.505\Delta$ in (c), as shown by the horizontal lines in Fig. 6.

Qualitatively, current-phase relation is similar for both types of Josephson junctions. As the quasi-Fermi energy

sweeps through the a bound Andreev level, the current-phase relation changes from sinusoidal, to a half-periodic relation, and finally to a π -phase shifted junction¹⁵. All these changes in the current-phase relation are similar to those occurring in ballistic SNS junctions.^{8,12}, including the half-periodic and π -phase shifted (sign change of the Josephson current) current-phase relations. The current-phase relation for the symmetric junction evolves from the usual sinusoidal form into a nearly linear variation of current with phase more typical of ballistic junctions. The half-periodic current-phase relation can be observed as a doubling of the AC Josephson frequency^{31,32}.

When we depopulate one of the Andreev levels with the probe voltage, we increase the magnitude of the critical current. The equilibrium Josephson current is a small difference between much larger positive and negative currents flowing in equilibrium. Depopulating an Andreev level removes some of this current cancellation in both the asymmetric and symmetric junction types, increas-

ing the Josephson critical current. However, the Andreev levels in the SIS junction with inversion symmetry carry a slightly larger current (by a factor of $\simeq 4$ in Fig. 6). There is a small difference between the Josephson current between applying positive and negative gate voltages not shown in Fig. 6, similar to Fig. 2(b) for the short junction, again due to a small leakage current from the gate.

IV. CONCLUSIONS

An additional normal metal terminal weakly coupled to a Josephson junction, permits one both to determine the Andreev energy levels and to probe the Josephson current carried through these bound levels. The differential conductance $dI_N(\phi, V)/dV$ along the normal metal probe determines the Andreev level positions and width, while changes in the Josephson current $I(\phi, V)$ as a function of the probe voltage determine the Andreev level currents. Setting the probe voltage above the energy gap also allows a measurement of the ‘continuum’ Josephson current, which flows outside the energy gap. In this paper we have studied the Josephson current switching and spectroscopy of the Andreev energy levels in a three terminal SIS junction, where the normal region of the Josephson junction also contains an insulator having transmission probability $T \leq 1$. The results are qualitatively different from the ballistic Josephson junction ($T = 1$) we considered in an earlier paper¹².

In a short Josephson junction ($L \ll \xi_0$) containing a tunnel barrier ($T \ll 1$), the maximum Josephson current switches from the Ambegaokar-Baratoff value ($e\Delta T/2\hbar$) to zero when the probe voltage is approximately the energy gap, $|eV| \simeq \Delta$. In a short junction, there are two Andreev levels which carry equal and opposite currents. Therefore, populating (or depopulating) both levels forces the Josephson current to zero. Since the presence of a tunnel barrier with $T \ll 1$ forces the Andreev levels to the gap edge at $E \simeq \pm\Delta$, the Josephson current switches to zero when $|eV| \simeq \Delta$ (independent of the phase difference). Although the magnitude of the change in the Josephson current is larger in ballistic junctions (approaching $e\Delta/\hbar$), the switching voltage in ballistic junctions ranges between $0 \leq eV \leq \Delta$ (depending on ϕ).

In a long Josephson junction ($L \gg \xi_0$) containing a tunnel barrier ($T \ll 1$), the details of this current switching depend on the scattering potential inside the normal region. For the long SIS junction having inversion symmetry, a current proportional to \sqrt{T} indeed flows through the junction²⁷ when one applies certain voltages to the normal metal probe. (The exact current is $ev_F/(L + 2\xi(E_n^\pm))\sqrt{T}$ where $\xi(E_n^\pm)$ is the energy dependent coherence length.) The factor of \sqrt{T} arises because the inversion symmetry allows degenerate energy levels

to exist even in the presence of a tunnel barrier, similar to the midgap states in d-wave superconductors.²⁹ Although this nonequilibrium current (proportional to \sqrt{T}) is much larger than the equilibrium Josephson tunneling current (proportional to T), both the changes in the nonequilibrium Josephson current and magnitude of the equilibrium current are much smaller in SIS junctions than for ballistic SNS junctions (which approach $ev_F/(L + 2\xi_0)$).

The bandwidth of the Andreev levels also becomes smaller with decreasing barrier transmission in long SIS junctions. The range of gate voltages for which one obtains a nonequilibrium current in the long SIS junction is equal to this bandwidth, namely $4\sqrt{T}\Delta(\xi_0/(L + 2\xi_0))$. There are approximately $(L + 2\xi_0)/2\pi\xi_0$ of these energy levels, so the total range of voltages over which the Josephson current differs significantly from equilibrium is $4\sqrt{T}\Delta/\pi$. Reducing the barrier transmission T to maximize the size of the nonequilibrium current simultaneously lowers the range of gate voltages over which one can observe this current. In a ballistic SNS junction, the Josephson current differs significantly from its equilibrium value over a much larger range of voltages $\Delta/2$, namely half of the energy gap. Nonequilibrium effects on the Josephson current from the additional normal metal probe are much larger and occur over a much broader range of gate voltage in ballistic SNS junctions.

For long SIS junctions which do not possess inversion symmetry, the energy gaps and currents carried by the Andreev levels are in general different, so that the Josephson current switches by different amounts whenever the gate voltage populates a new Andreev level. The magnitude of the Josephson current switching can range between the equilibrium value of the current (proportional to T) and the larger nonequilibrium currents found in symmetric junctions (proportional to \sqrt{T}). If only a very small energy gap occurs near an Andreev level crossing, main features of the Josephson current switching and spectroscopy of the Andreev levels are qualitatively similar to the symmetric junctions. But because the Andreev levels carry different currents in general, the cancellation between currents flowing in opposite directions from two levels adjacent in energy is almost never exact. The Josephson current can differ from its equilibrium value over a much wider range of gate voltages in long and asymmetric SIS junctions.

V. ACKNOWLEDGEMENTS

We thank Manoj Samanta for many useful discussions. We gratefully acknowledge support from the MRSEC of the National Science Foundation under grant No. DMR-9400415 (PFB).

APPENDIX A: SCATTERING STATES

We compute the Josephson current by finding both the scattering state and bound state solutions of the BdG equation

$$\begin{pmatrix} H(x) - \mu & \Delta(x) \\ \Delta^*(x) & -(H^*(x) - \mu) \end{pmatrix} \begin{pmatrix} u(x) \\ v(x) \end{pmatrix} = E \begin{pmatrix} u(x) \\ v(x) \end{pmatrix} . \quad (A1)$$

For our model Josephson junction we take the Hamiltonian

$$H(x) = -\frac{\hbar^2}{2m} \frac{d^2}{dx^2} + V(x) , \quad (A2)$$

the scattering potential

$$V(x) = V_s \delta(x - a) , \quad (A3)$$

where $0 \leq a \leq L$, and pair potential

$$\Delta(x) = \begin{cases} \Delta e^{i\phi_1} & x < 0 \\ 0 & 0 < x < L \\ \Delta e^{i\phi_2} & x > L \end{cases} . \quad (A4)$$

We first obtain the solutions of Eq. (A1) in a uniform superconductor where $\Delta(x) = \text{constant}$ and $V(x) = \text{constant}$. When the pair potential and electrostatic potential vary in space, we determine the scattering state solutions of Eq. (A1) by matching quasiparticle wave amplitudes at the potential discontinuities at $x = 0, x = a, x = b$ and $x = L$ as shown in Fig. 7. We essentially follow the calculational methods outlined in the Appendices of Refs.⁹ and¹².

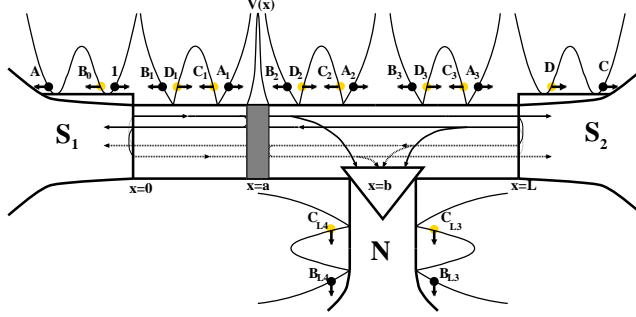


FIG. 7. An electron-like quasiparticle is injected from the the left superconductor reservoir. The wave amplitude described by B_0 represents the term $B - \frac{u_0}{v_0}$ in Eq. A5. The wave amplitudes in the right superconductor can be obtained in terms of A and B by matching the boundary conditions at $x = 0, x = a, x = b$ and $x = L$.

Fig. 7 illustrates an electronlike quasi-particle injected from the left superconducting reservoir. In the Andreev approximation, an electron like excitation incident from the left superconductor ($x < 0$) generates both reflected and transmitted quasi-particles described by the wave function

$$\begin{pmatrix} u_0 e^{i\phi_1} \\ v_0 \end{pmatrix} e^{ik_e x} + \left[B - \frac{u_0}{v_0} \right] \begin{pmatrix} v_0 e^{i\phi_1} \\ u_0 \end{pmatrix} e^{ik_h x} + A \begin{pmatrix} u_0 e^{i\phi_1} \\ v_0 \end{pmatrix} e^{-ik_e x} , \quad (A5)$$

valid for ($x \geq 0 \leq a$). In Eq. (A5), the first term represents the electronlike quasiparticle injected from the left superconducting reservoir. The term denoted by the coefficient A describes the electron-like particle normally reflected from the impurity while the term denoted by the coefficient B describes the Andreev reflected hole-like quasi-particle. The transmitted electron-like quasiparticle and the Andreev reflected hole-like quasiparticle in the right superconductor ($x > L$) have the wave function

$$C \begin{pmatrix} u_0 e^{i\phi_2} \\ v_0 \end{pmatrix} e^{ik_e(x - L)} + D \begin{pmatrix} v_0 e^{i\phi_2} \\ u_0 \end{pmatrix} e^{-ik_h(x - L)} . \quad (A6)$$

The term with the coefficient D describes the hole-like normal reflections from the impurity which are first Andreev reflected from the right superconductor. The BCS coherence factors u_0 and v_0 in Eqs. (A5)-(A6) are

$$2u_0^2 = 1 + \frac{\sqrt{E^2 - \Delta^2}}{|E|}, \quad (\text{A7})$$

and

$$2v_0^2 = 1 - \frac{\sqrt{E^2 - \Delta^2}}{|E|}. \quad (\text{A8})$$

The wave vectors k_e and k_h in Eqs. (A5)-(A6) are

$$k_e = \sqrt{\frac{2m}{\hbar^2} \left(\mu + \sqrt{E^2 - \Delta^2} \right)}, \quad (\text{A9})$$

and

$$k_h = \sqrt{\frac{2m}{\hbar^2} \left(\mu - \sqrt{E^2 - \Delta^2} \right)}. \quad (\text{A10})$$

As shown in Fig. 7., quasi-particle waves inside the normal region are grouped into three sets. We obtain the quasiparticle wave function in the normal regions ($b < x < L$) and ($0 < x < a$) by matching the waves at pair potential interfaces $x = L$ and $x = 0$ respectively. Therefore, for electrons in region ($0 < x < a$) we have

$$A_1 \begin{pmatrix} 1 \\ 0 \end{pmatrix} e^{i\tilde{k}_e x} + C_1 \begin{pmatrix} 0 \\ 1 \end{pmatrix} e^{i\tilde{k}_h x} = \begin{pmatrix} Bv_0 e^{i\phi_1} \\ 0 \end{pmatrix} e^{i\tilde{k}_e x} + \begin{pmatrix} 0 \\ (B - \frac{u_0}{v_0} + \frac{v_0}{u_0})u_0 \end{pmatrix} e^{i\tilde{k}_h x}. \quad (\text{A11})$$

Similarly, in region ($b < x < L$), matching the wave functions yields

$$A_3 \begin{pmatrix} 1 \\ 0 \end{pmatrix} e^{i\tilde{k}_e(x-b)} + C_3 \begin{pmatrix} 0 \\ 1 \end{pmatrix} e^{i\tilde{k}_h(x-b)} = \begin{pmatrix} Cu_0 e^{i\phi_2} e^{-i\tilde{k}_e(L-b)} \\ 0 \end{pmatrix} e^{i\tilde{k}_e(x-b)} + \begin{pmatrix} 0 \\ Cu_0 e^{-i\tilde{k}_h(L-b)} \end{pmatrix} e^{i\tilde{k}_h(x-b)}. \quad (\text{A12})$$

For holes in region ($0 < x < a$) we obtain

$$B_1 \begin{pmatrix} 1 \\ 0 \end{pmatrix} e^{-i\tilde{k}_e x} + D_1 \begin{pmatrix} 0 \\ 1 \end{pmatrix} e^{-i\tilde{k}_h x} = \begin{pmatrix} Au_0 e^{i\phi_1} \\ 0 \end{pmatrix} e^{-i\tilde{k}_e x} + \begin{pmatrix} 0 \\ Av_0 \end{pmatrix} e^{-i\tilde{k}_h x}, \quad (\text{A13})$$

and in region ($b < x < L$) we have

$$B_3 \begin{pmatrix} 1 \\ 0 \end{pmatrix} e^{-i\tilde{k}_e(x-b)} + D_3 \begin{pmatrix} 0 \\ 1 \end{pmatrix} e^{-i\tilde{k}_h(x-b)} = \begin{pmatrix} Dv_0 e^{i\phi_2} e^{i\tilde{k}_e(L-b)} \\ 0 \end{pmatrix} e^{-i\tilde{k}_e(x-b)} + \begin{pmatrix} 0 \\ Du_0 e^{i\tilde{k}_h(L-b)} \end{pmatrix} e^{-i\tilde{k}_h(x-b)}. \quad (\text{A14})$$

Since pair potential Δ is zero in the normal region, the wave vectors \tilde{k}_e and \tilde{k}_h in Eq. (A11)-(A14) are obtained from Eq. (A9) and (A10) by setting $\Delta = 0$.

The current amplitudes of incoming and outgoing waves at the impurity ($x = a$) and at the normal-metal side probe ($x = b$) are connected via two separate scattering matrices. The scattering matrix for electrons at $x = a$ is

$$\begin{pmatrix} A_2 \\ B_1 e^{-i\tilde{k}_e a} \end{pmatrix} = \begin{pmatrix} t(\tilde{k}_e) & r(\tilde{k}_e) \\ r(\tilde{k}_e) & t(\tilde{k}_e) \end{pmatrix} \begin{pmatrix} A_1 e^{i\tilde{k}_e a} \\ B_2 \end{pmatrix}. \quad (\text{A15})$$

Similarly, for holes at $x = a$, the scattering matrix is

$$\begin{pmatrix} C_1 e^{\tilde{k}_h a} \\ D_2 \end{pmatrix} = \begin{pmatrix} t^*(\tilde{k}_h) & r^*(\tilde{k}_h) \\ r^*(\tilde{k}_h) & t^*(\tilde{k}_h) \end{pmatrix} \begin{pmatrix} C_2 \\ D_1 e^{-i\tilde{k}_h a} \end{pmatrix}. \quad (\text{A16})$$

The current transmission and reflection amplitudes for the point scatterer matrices in Eqs. (A15)-(A16) are

$$t(k) = \frac{1}{1 + i(mV_s/\hbar^2 k)} \quad (A17)$$

and

$$r(k) = \frac{-i(mV_s/\hbar^2 k)}{1 + i(mV_s/\hbar^2 k)} \quad (A18)$$

At $x = b$ the quasiparticle wave amplitudes are coupled by another scattering matrix to the normal-metal side probe. Since we assumed that the normal-metal probe only breaks the phase of a quasi-particle, but not its momentum, we conceptually view the normal probe as two separate leads. We couple right-moving quasi-particles only to lead 3 while the left-moving quasi-particles to lead 4. Therefore, the scattering matrix becomes

$$\mathbf{S} = \begin{pmatrix} 0 & \sqrt{1-\epsilon} & \sqrt{\epsilon} & 0 \\ \sqrt{1-\epsilon} & 0 & 0 & -\sqrt{\epsilon} \\ \sqrt{\epsilon} & 0 & 0 & \sqrt{1-\epsilon} \\ 0 & \sqrt{\epsilon} & -\sqrt{1-\epsilon} & 0 \end{pmatrix}. \quad (A19)$$

The scattering matrix \mathbf{S} from Eq. (A19) relates the current amplitudes for electrons in normal region ($a < x < b$) and normal region ($b < x < L$) as

$$\begin{pmatrix} A_3 \\ B_2 e^{-i\tilde{k}_e(b-a)} \\ B_{L4} \\ B_{L3} \end{pmatrix} = (\mathbf{S}) \begin{pmatrix} B_3 \\ A_2 e^{i\tilde{k}_e(b-a)} \\ 0 \\ 0 \end{pmatrix}. \quad (A20)$$

The current amplitudes for holes, in the same regions are related as

$$\begin{pmatrix} C_2 e^{i\tilde{k}_h(b-a)} \\ D_3 \\ C_{L4} \\ C_{L3} \end{pmatrix} = (\mathbf{S}) \begin{pmatrix} D_3 e^{-i\tilde{k}_h(b-a)} \\ C_3 \\ 0 \\ 0 \end{pmatrix}. \quad (A21)$$

By combining Eqs. (A5), (A6), (A11), (A12), (A13), (A14), (A15), (A16), (A20), and (A21) we obtain matrix equations for the coefficients C and D as

$$\begin{pmatrix} \frac{v_0}{u_0} \\ r(\tilde{k}_e) \end{pmatrix} \begin{pmatrix} t(\tilde{k}_e) & r(\tilde{k}_e) \\ r(\tilde{k}_e) & t(\tilde{k}_e) \end{pmatrix} \begin{pmatrix} e^{i(\tilde{k}_e - \tilde{k}_h)a} & 0 \\ 0 & (1-\epsilon)e^{i\phi} e^{-i(\tilde{k}_e - \tilde{k}_h)(a-L)} \end{pmatrix} X \quad (A22)$$

$$\begin{pmatrix} \frac{v_0}{u_0} \\ r^*(\tilde{k}_h) \end{pmatrix} \begin{pmatrix} t^*(\tilde{k}_h) & r^*(\tilde{k}_h) \\ r^*(\tilde{k}_h) & t^*(\tilde{k}_h) \end{pmatrix} \begin{pmatrix} (1-\epsilon)e^{-i(\tilde{k}_e - \tilde{k}_h)(a-L)} e^{-i\phi} & 0 \\ 0 & e^{i(\tilde{k}_e - \tilde{k}_h)a} \end{pmatrix} \begin{pmatrix} C' \\ A' \end{pmatrix}$$

$$+ \begin{pmatrix} \left(\frac{v_0}{u_0} - \frac{v_0}{u_0}\right) e^{i\tilde{k}_h a} \\ 0 \end{pmatrix} \Big\} = \begin{pmatrix} 1 & 0 \\ 0 & 1 \end{pmatrix} \begin{pmatrix} C' \\ A' \end{pmatrix}. \quad (A23)$$

and

$$\begin{pmatrix} \frac{v_0}{u_0} \\ r^*(\tilde{k}_h) \end{pmatrix}^2 \begin{pmatrix} t^*(\tilde{k}_h) & r^*(\tilde{k}_h) \\ r^*(\tilde{k}_h) & t^*(\tilde{k}_h) \end{pmatrix} \begin{pmatrix} (1-\epsilon)e^{-i(\tilde{k}_e - \tilde{k}_h)(a-L)} e^{-i\phi} & 0 \\ 0 & e^{i(\tilde{k}_e - \tilde{k}_h)a} \end{pmatrix} X$$

$$\begin{pmatrix} t(\tilde{k}_e) & r(\tilde{k}_e) \\ r(\tilde{k}_e) & t(\tilde{k}_e) \end{pmatrix} \begin{pmatrix} e^{i(\tilde{k}_e - \tilde{k}_h)a} & 0 \\ 0 & (1-\epsilon)e^{-i(\tilde{k}_e - \tilde{k}_h)(a-L)} e^{i\phi} \end{pmatrix} \begin{pmatrix} B' \\ D' \end{pmatrix}$$

$$+ \begin{pmatrix} \left(\frac{u_0}{v_0} - \frac{u_0}{v_0}\right) e^{i\tilde{k}_h a} \\ 0 \end{pmatrix} = \begin{pmatrix} 1 & 0 \\ 0 & 1 \end{pmatrix} \begin{pmatrix} B' \\ D' \end{pmatrix}. \quad (A24)$$

In Eqs. (A23), the C' , A' , B' , D' are related to C , A , B , D through

$$C' = \frac{Ce^{i\phi}e^{-i\tilde{k}_e(L-a)}}{\sqrt{1-\epsilon}} \quad , \quad (A25)$$

$$A' = Ae^{-i\tilde{k}_e a} \quad , \quad (A26)$$

$$B' = Be^{i\tilde{k}_h a} \quad , \quad (A27)$$

and

$$D' = \frac{De^{i\tilde{k}_h(L-a)}}{\sqrt{1-\epsilon}} \quad . \quad (A28)$$

Finally, by inverting the matrix equations (A23)-(A28), we can directly obtain the scattering amplitudes as

$$C_{1 \rightarrow 2}^e = t \frac{\left(1 - \left(\frac{v_0}{u_0}\right)^2 (1-\epsilon)e^{i\phi}e^{i(\tilde{k}_e - \tilde{k}_h)L}\right) \sqrt{1-\epsilon} \left(1 - \left(\frac{v_0}{u_0}\right)^2\right) e^{-i\phi}e^{i\tilde{k}_e L}}{F(\phi, \epsilon, T)} \quad , \quad (A29)$$

and

$$D_{1 \rightarrow 2}^e = \frac{\left(\frac{v_0}{u_0}\right) \left(1 - \left(\frac{v_0}{u_0}\right)^2\right) \left(tr^*(1-\epsilon)e^{-i\phi}e^{i(\tilde{k}_e - \tilde{k}_h)(L-a)} + rt^*e^{i(\tilde{k}_e - \tilde{k}_h)a}\right) \sqrt{1-\epsilon} e^{-i\tilde{k}_h(L-a)} e^{i\tilde{k}_e a}}{F(\phi, \epsilon, T)} \quad . \quad (A30)$$

The resonant denominator $F(\phi, \epsilon, T)$, whose zeroes give the position and width of the Andreev resonances, is

$$F(\phi, \epsilon, T) = 1 - 2T(1-\epsilon) \left(\frac{v_0}{u_0}\right)^2 e^{i(\tilde{k}_e - \tilde{k}_h)L} \cos \phi - R \left(\frac{v_0}{u_0}\right)^2 e^{2i(\tilde{k}_e - \tilde{k}_h)a} - R(1-\epsilon)^2 \left(\frac{v_0}{u_0}\right)^2 e^{2i(\tilde{k}_e - \tilde{k}_h)(L-a)} + (1-\epsilon)^2 \left(\frac{v_0}{u_0}\right)^4 e^{2i(\tilde{k}_e - \tilde{k}_h)L} \quad . \quad (A31)$$

For any other quasiparticle, injected from either superconducting contacts or "conceptual" normal probes, one can obtain the wave-function amplitudes by calculations similar to the ones described above. In Appendix B we outline the derivation of the electrical current flowing into the right superconductor from those wave-function amplitudes.

APPENDIX B: ELECTRICAL CURRENT

The electrical current flow in the right superconductor due to the injection of a quasiparticle from any lead is³⁰

$$I_2 = \sum_{k;q\beta} (J_u + J_v)_{q \rightarrow 2}^\beta f_q^\beta - \sum_{k;q\beta} (J_v)_{q \rightarrow 2}^\beta \quad . \quad (B1)$$

We use the indices $q = 1, 2, 3, 4$ as the lead numbers, k as the wave number of the injected quasi-particle, and $\beta = (e \text{ or } h)$ denotes the injection of electron-like or hole-like quasi-particles. The J_u and J_v are the Schrödinger currents carried by the waves u and v , namely,

$$J_u = (e\hbar/m)\text{Im}\{u^*(x)\nabla u(x)\} \quad , \quad (B2)$$

and

$$J_v = (e\hbar/m)\text{Im}\{v^*(x)\nabla v(x)\} \quad . \quad (B3)$$

The last term in Eq. (B1), $\sum_{k;q\beta} (J_v)_{q \rightarrow 2}^\beta = 0$, is called ‘vacuum current’ and is zero in DC problems.

We can now define the transmission coefficients $T_{q \rightarrow 2}^\beta$, which give the ratio of electrical current out to particle current in, as

$$ev_F T_{q \rightarrow 2}^\beta = (J_u + J_v)_{q \rightarrow 2}^\beta , \quad (B4)$$

where $v_F = \hbar k_F/m$. Equation (B1) then reduces to

$$I_p = e \sum_{k;q\beta} v_F T_{q \rightarrow 2}^\beta f_q^\beta , \quad (B5)$$

which is the standard Landauer-Büttiker form. The Fermi factor f_q^β in Eq. (B5) is

$$f_q^\beta = f(E - eV_q^\beta) , \quad (B6)$$

where eV_q^β is the effective biasing voltage applied to the q th lead. Since we ground both superconducting leads, we have $eV_1^\beta = eV_2^\beta = 0$. The effective biasing voltages applied to the normal-metal leads are

$$eV_3^e = eV_4^e = eV , \quad (B7)$$

$$eV_3^h = eV_4^h = -eV . \quad (B8)$$

We obtain the current flow into the right superconductor by converting the sum over k in Eq. (B5) into an integral over the injected energies, namely

$$\begin{aligned} I_2(\phi, \epsilon, V, T) = & e \left(\int_{-\infty}^{-\Delta} + \int_{\Delta}^{\infty} \right) v_F N_s^+(E) [T_{1 \rightarrow 2}^e + T_{1 \rightarrow 2}^h + T_{2 \rightarrow 2}^e + T_{2 \rightarrow 2}^h] f(E) dE \\ & + e \int_{-\infty}^{\infty} v_F N_n^+(E) [T_{3 \rightarrow 2}^e + T_{4 \rightarrow 2}^e] f(E - eV) dE \\ & + e \int_{-\infty}^{\infty} v_F N_n^+(E) [T_{3 \rightarrow 2}^h + T_{4 \rightarrow 2}^h] f(E + eV) dE , \end{aligned} \quad (B9)$$

where the superconducting density of states $N_s^+(E)$ related to the normal density of states $N_n^+(E)$ by

$$N_s^+(E) = \frac{1}{|u_0^2 - v_0^2|} N_n^+(E) . \quad (B10)$$

Combining the identity $v_F N_s^+(E) \simeq 1/h$, along with Eqs. (B9)-(B10), we obtain

$$\begin{aligned} I_2(\phi, \epsilon, V, T) = & \frac{e}{h} \left(\int_{-\infty}^{-\Delta} + \int_{\Delta}^{\infty} \right) [T_{1 \rightarrow 2}^e + T_{1 \rightarrow 2}^h + T_{2 \rightarrow 2}^e + T_{2 \rightarrow 2}^h] f(E) dE \\ & + \frac{e}{h} \int_{-\infty}^{\infty} [T_{3 \rightarrow 2}^e + T_{4 \rightarrow 2}^e] f(E - eV) dE \\ & + \frac{e}{h} \int_{-\infty}^{\infty} [T_{3 \rightarrow 2}^h + T_{4 \rightarrow 2}^h] f(E + eV) dE , \end{aligned} \quad (B11)$$

The transmission coefficients T in Eq. (B11) are related simply to the scattering amplitudes calculated in Appendix A. Using Eq. (B2), (B3), (B5) and (A6) we obtain $T_{1 \rightarrow 2}^e$, for example, as

$$T_{1 \rightarrow 2}^e = |C_{1 \rightarrow 2}^e|^2 - |D_{1 \rightarrow 2}^e|^2 . \quad (B12)$$

The other transmission coefficients and wave-function amplitudes can be obtained by calculations similar to the one in Appendix A. Hence for a hole-like quasiparticle injected from the left superconductor we have

$$T_{1 \rightarrow 2}^h = |C_{1 \rightarrow 2}^h|^2 - |D_{1 \rightarrow 2}^h|^2 , \quad (B13)$$

where

$$C_{1 \rightarrow 2}^h = \left(\frac{v_0}{u_0} \right) \left(1 - \left(\frac{v_0}{u_0} \right)^2 \right) X \frac{\left(t^* r (1 - \epsilon) e^{i\phi} e^{i(\tilde{k}_e - \tilde{k}_h)(L - a)} + r^* t e^{i(\tilde{k}_e - \tilde{k}_h)a} \right) \sqrt{1 - \epsilon} e^{-i\tilde{k}_h a} e^{-i\phi} e^{i\tilde{k}_e(L - a)}}{F(\phi, \epsilon, T)}, \quad (B14)$$

and

$$D_{1 \rightarrow 2}^h = t^* \frac{\left(1 - \left(\frac{v_0}{u_0} \right)^2 (1 - \epsilon) e^{-i\phi} e^{i(\tilde{k}_e - \tilde{k}_h)L} \right) \left(1 - \left(\frac{v_0}{u_0} \right)^2 \right) \sqrt{(1 - \epsilon)} e^{-i\tilde{k}_h L}}{F(\phi, \epsilon, T)}. \quad (B15)$$

For an electron-like quasiparticle injected from the right superconductor we find the transmission probability

$$T_{2 \rightarrow 2}^e = -1 + |C_{2 \rightarrow 2}^e|^2 - |D_{2 \rightarrow 2}^e|^2 - (4u_0 v_0 - 2 \frac{u_0}{v_0}) \text{Re}\{D_{2 \rightarrow 2}^e\} - \frac{u_0^2}{v_0^2} + 4u_0^2, \quad (B16)$$

where

$$C_{2 \rightarrow 2}^e = r \frac{\left(1 - \left(\frac{v_0}{u_0} \right)^2 e^{2i(\tilde{k}_e - \tilde{k}_h)a} \right) \left(1 - \left(\frac{v_0}{u_0} \right)^2 \right) (1 - \epsilon) e^{2i\tilde{k}_e(L - a)}}{F(\phi, \epsilon, T)}, \quad (B17)$$

and

$$D_{2 \rightarrow 2}^e = \frac{\left(1 - \left(\frac{v_0}{u_0} \right)^2 [T(1 - \epsilon) e^{-i\phi} e^{i(\tilde{k}_e - \tilde{k}_h)L} + R e^{2i(\tilde{k}_e - \tilde{k}_h)a}] \right) \left(1 - \left(\frac{v_0}{u_0} \right)^2 \right) \left(\frac{u_0}{v_0} \right)}{F(\phi, \epsilon, T)}. \quad (B18)$$

For a hole-like quasiparticle incident from right superconductor, we find

$$T_{2 \rightarrow 2}^h = 1 - |C_{2 \rightarrow 2}^h|^2 + |D_{2 \rightarrow 2}^h|^2 + (4u_0 v_0 - 2 \frac{u_0}{v_0}) \text{Re}\{D_{2 \rightarrow 2}^h\} + \frac{u_0^2}{v_0^2} - 4u_0^2, \quad (B19)$$

where

$$C_{2 \rightarrow 2}^h = \frac{\left(1 - \left(\frac{v_0}{u_0} \right)^2 [T(1 - \epsilon) e^{i\phi} e^{i(\tilde{k}_e - \tilde{k}_h)L} + R e^{2i(\tilde{k}_e - \tilde{k}_h)a}] \right) \left(1 - \left(\frac{v_0}{u_0} \right)^2 \right) \left(\frac{u_0}{v_0} \right)}{F(\phi, \epsilon, T)}, \quad (B20)$$

and

$$D_{2 \rightarrow 2}^h = r^* \frac{\left(1 - \left(\frac{v_0}{u_0} \right)^2 e^{2i(\tilde{k}_e - \tilde{k}_h)a} \right) \left(1 - \left(\frac{v_0}{u_0} \right)^2 \right) (1 - \epsilon) e^{2i\tilde{k}_h(L - a)}}{F(\phi, \epsilon, T)}. \quad (B21)$$

For an electron-like quasiparticle injected from the normal probe in channel 3 we have

$$T_{3 \rightarrow 2}^e = |C_{3 \rightarrow 2}^e|^2 - |D_{3 \rightarrow 2}^e|^2, \quad (B22)$$

where

$$C_{3 \rightarrow 2}^e = r \frac{\left(1 - \left(\frac{v_0}{u_0} \right)^2 e^{2i(\tilde{k}_e - \tilde{k}_h)a} \right) \sqrt{|u_0|^2 + |v_0|^2} \sqrt{\epsilon(1 - \epsilon)} e^{-i\phi_2} e^{i\tilde{k}_h(L + b - 2a)}}{u_0 F(\phi, \epsilon, T)}, \quad (B23)$$

and

$$D_{3 \rightarrow 2}^e = \left(\frac{v_0}{u_0} \right) \sqrt{|u_0|^2 + |v_0|^2} \sqrt{\epsilon(1-\epsilon)} e^{-i\phi_2} e^{i\tilde{k}_e(b-a)} e^{-i\tilde{k}_h(L-a)} \frac{\left(R(1-\epsilon) e^{i(\tilde{k}_e - \tilde{k}_h)(L-a)} + T e^{i\phi} e^{i(\tilde{k}_e - \tilde{k}_h)a} - \left(\frac{v_0}{u_0} \right)^2 (1-\epsilon) e^{i(\tilde{k}_e - \tilde{k}_h)(L+a)} \right)}{u_0 F(\phi, \epsilon, T)}. \quad (B24)$$

For a hole-like quasiparticle incident from the normal probe in channel 3 we have

$$T_{3 \rightarrow 2}^h = |D_{3 \rightarrow 2}^h|^2 - |C_{3 \rightarrow 2}^h|^2, \quad (B25)$$

where

$$C_{3 \rightarrow 2}^h = \left(\frac{v_0}{u_0} \right) \sqrt{|u_0|^2 + |v_0|^2} \sqrt{\epsilon(1-\epsilon)} e^{-i\tilde{k}_h(b-a)} e^{i\tilde{k}_e(L-a)} \frac{\left(R(1-\epsilon) e^{i(\tilde{k}_e - \tilde{k}_h)(L-a)} + T e^{-i\phi} e^{i(\tilde{k}_e - \tilde{k}_h)a} - \left(\frac{v_0}{u_0} \right)^2 (1-\epsilon) e^{i(\tilde{k}_e - \tilde{k}_h)(L+a)} \right)}{u_0 F(\phi, \epsilon, T)}. \quad (B26)$$

and

$$D_{3 \rightarrow 2}^h = r^* \frac{\left(1 - \left(\frac{v_0}{u_0} \right)^2 e^{2i(\tilde{k}_e - \tilde{k}_h)a} \right) \sqrt{|u_0|^2 + |v_0|^2} \sqrt{\epsilon(1-\epsilon)} e^{-i\tilde{k}_h(L+b-2a)}}{u_0 F(\phi, \epsilon, T)}. \quad (B27)$$

For an electron-like quasiparticle injected from the normal probe in channel 4 we have

$$T_{4 \rightarrow 2}^e = |C_{4 \rightarrow 2}^e|^2 - |D_{4 \rightarrow 2}^e|^2, \quad (B28)$$

where

$$C_{4 \rightarrow 2}^e = \sqrt{|u_0|^2 + |v_0|^2} \sqrt{\epsilon} \frac{\left(1 - \left(\frac{v_0}{u_0} \right)^2 [Re^{2i(\tilde{k}_e - \tilde{k}_h)a} + T(1-\epsilon) e^{i\phi} Re^{i(\tilde{k}_e - \tilde{k}_h)L}] \right) e^{-i\phi_2} e^{i\tilde{k}_e(L-b)}}{u_0 F(\phi, \epsilon, T)}, \quad (B29)$$

and

$$D_{4 \rightarrow 2}^e = r^* \frac{\left(\frac{v_0}{u_0} \right) \sqrt{|u_0|^2 + |v_0|^2} \sqrt{\epsilon(1-\epsilon)} \left(1 - \left(\frac{v_0}{u_0} \right)^2 e^{2i(\tilde{k}_e - \tilde{k}_h)a} \right) e^{-i\phi_2} e^{i\tilde{k}_e(L-b)} e^{-2i\tilde{k}_h(L-a)}}{u_0 F(\phi, \epsilon, T)}. \quad (B30)$$

For a hole-like quasiparticle incident from the normal probe in channel 4 we have

$$T_{4 \rightarrow 2}^h = |C_{4 \rightarrow 2}^h|^2 - |D_{4 \rightarrow 2}^h|^2, \quad (B31)$$

where

$$C_{4 \rightarrow 2}^h = r \left(\frac{v_0}{u_0} \right) \sqrt{|u_0|^2 + |v_0|^2} \sqrt{\epsilon(1-\epsilon)} \frac{\left(1 - \left(\frac{v_0}{u_0} \right)^2 e^{2i(\tilde{k}_e - \tilde{k}_h)a} \right) e^{-i\tilde{k}_h(L-b)} e^{2i\tilde{k}_e(L-a)}}{u_0 F(\phi, \epsilon, T)}, \quad (B32)$$

and

$$D_{4 \rightarrow 2}^h = \frac{\sqrt{|u_0|^2 + |v_0|^2} \sqrt{\epsilon}}{u_0 F(\phi, \epsilon, T)} \frac{\left(1 - \left(\frac{v_0}{u_0} \right)^2 [Re^{2i(\tilde{k}_e - \tilde{k}_h)a} + T(1 - \epsilon)e^{-i\phi} e^{i(\tilde{k}_e - \tilde{k}_h)L}] \right) e^{-i\tilde{k}_h(L - b)}}{u_0 F(\phi, \epsilon, T)}. \quad (B33)$$

¹ A.F. Andreev, 'The Thermal Conductivity of the Intermediate State in Superconductors', *Zh. Eksp. Teor. Fiz.*, **46**, 1823 (1964). [Soviet Physics JETP, **19**, 1228 (1964)] A.F. Andreev, 'Electron Spectrum of the Intermediate State in Superconductors', *Zh. Eksp. Teor. Fiz.*, **49**, 655 (1966). [Soviet Physics JETP, **22**, 455 (1966)]

² I.O. Kulik, 'Macroscopic Quantization and the Proximity Effect in S-N-S Junctions', *Zh. Eksp. Teor. Fiz.*, **57**, 1745 (1969). [Soviet Physics JETP, **30**, 944 (1970)]

³ C. Ishii, 'Josephson Currents Through Junctions with Normal Metal Barriers', *Progress of Theoretical Physics*, **44**, 1525 (1970). (See Eq. 3.21 and Fig. 5.)

⁴ J. Bardeen and J.L. Johnson, 'Josephson Current Flow in Pure Superconducting-Normal-Superconducting Junctions', *Phys. Rev. B*, **5**, 72 (1972).

⁵ I.O. Kulik and A.N. Omel'yanchuk, 'Properties of Superconducting Microbridges in the Pure Limit', *Fiz. Nizk. Temp.*, **3**, 945 (1977). [Soviet Journal of Low Temperature Physics, **3**, 459 (1977)] I.O. Kulik and A.N. Omel'yanchuk, 'Josephson Effect in Superconductive Bridges: Microscopic Theory', *Fiz. Nizk. Temp.*, **4**, 296 (1978). [Soviet Journal of Low Temperature Physics, **4**, 142 (1978)]

⁶ C.W.J. Beenakker and H. van Houten, 'Josephson Current Through a Superconducting Quantum Point Contact Shorter than the Coherence Length', *Physical Review Letters*, **66**, 3056 (1991).

⁷ A. Furusaki, H. Takayanagi, and M. Tsukada, 'Theory of Quantum Conduction of Supercurrent Through a Constriction', *Physical Review Letters*, **67**, 132 (1991). A. Furusaki, H. Takayanagi, and M. Tsukada, 'Josephson Effect of the Superconducting Quantum Point Contact', *Physical Review B*, **45**, 10563 (1992).

⁸ B.J. van Wees, K.M.H. Lenssen, and C.J.P.M. Harmans, 'Transmission Formalism for Supercurrent Flow in Multiprobe Superconductor-Semiconductor-Superconductor Devices', *Physical Review B*, **44**, 470 (1991).

⁹ P.F. Bagwell, 'Suppression of the Josephson Current Through a Narrow, Mesoscopic Semiconductor Channel by a Single Impurity', *Physical Review B*, **46**, 12573 (1992).

¹⁰ A.F. Morpurgo, T.M. Klapwijk, and B.J. van Wees, 'Hot Electron Tunable Supercurrent', *Appl. Phys. Lett.* **72**, 966 (1997).

¹¹ Th. Schäpers, J. Malindretos, J. Neurohr, S. Lacnenmann, A.A. Golubov, A. van der Hart, G. Crecelius, H. Hardtdegen, and H. Lüth, 'Demonstration of a current-controlled 3-terminal Nb-In_xGa_{1-x}As/InP Josephson contact', submitted to *Appl. Phys. Lett.* .

¹² L. Chang and P.F. Bagwell, 'Control of Andreev Level Occupation in a Josephson Junction by a Normal Metal Probe', *Physical Review B*, **55**, 12678 (1997).

¹³ P. Samuelsson, V.S. Shumeiko, and G. Wendin, 'Long-range Josephson effect in mesoscopic T-shaped Superconductor - Normal Metal - Superconductor Junctions', *Physical Review B*, **56**, R5763 (1997).

¹⁴ A.F. Volkov, 'New Phenomena in Josephson SINIS Junctions', *Phys. Rev. Lett.*, **74**, 4730 (1995).

¹⁵ F.K. Wilhelm, G. Schön, and A.D. Zaikin, 'The Mesoscopic SNS Transistor', preprint cond-mat/9803091.

¹⁶ H.T. Ilhan and P.F. Bagwell, 'Supercurrent switching in Three- and Four- Terminal Josephson Junctions', preprint cond-mat/9806263.

¹⁷ M.C. Koops, G.V. van Duyneveldt, and R. de Bruyn Ouboter, 'Direct Observation of the Current-Phase Relation of an Adjustable Superconducting Point Contact', *Phys. Rev. Lett.*, **77**, 2542 (1996).

¹⁸ E.L. Wolf, *Principles of Electron Tunneling Spectroscopy*, (Oxford, New York, 1985).

¹⁹ V. Ambegaokar and A. Baratoff, 'Tunneling Between Superconductors', *Physical Review Letters*, **10**, 486 (1963). See also the Errata, *Physical Review Letters*, **11**, 104 (1963).

²⁰ W. Haberkorn, H. Knauer, and J. Richter, 'A Theoretical Study of the Current-Phase Relation in Josephson Contacts', *Phys. Stat. Sol.*, **47**, K161 (1978).

²¹ A.V. Zaitsev, 'Quasiclassical Equations of the Theory of Superconductivity for Contiguous Metals and the Properties of Constricted Microcontacts', *Zh. Eksp. Teor. Fiz.*, **86**, 1742 (1984). [Sov. Phys. JETP, **59**, 1015 (1984)]

²² G.B. Arnold, 'Superconducting Tunneling Without the Tunneling Hamiltonian', *J. of Low Temperature Physics*, **59**, 143 (1985).

²³ L.I. Glazman and K.A. Matveev, 'Resonant Josephson Current Through Kondo Impurities in a Tunnel Barrier', *Pis'ma Zh. Eksp. Teor. Fiz.*, **49**, 570 (1989). [JETP Letters, **49**, 659 (1989)] See Eq. (5).

²⁴ A. Furusaki and M. Tsukada, 'A Unified Theory of Clean Josephson Junctions', *Physica B*, **165 & 166**, 967 (1990).

²⁵ C.W.J. Beenakker, 'Universal Limit of Critical Current Fluctuations in Mesoscopic Josephson Junctions', *Physical Review Letters*, **67**, 3836 (1991).

²⁶ A.V. Svidzinski, T.N. Antsygina, and E.N. Bratus', 'Superconducting Current in Wide SNS Junctions', *Zh. Eksp. Teor. Fiz.*, **61**, 1612 (1971). [Sov. Phys. JETP, **34**, 860 (1972)] A.V. Svidzinski, T.N. Antsygina, and E.N. Bratus', 'Concerning the Theory of the Josephson Effect in Pure SNS Junctions', *Journal of Low Temperature Physics*, **10**, 131 (1973).

²⁷ G. Wendin and V.S. Shumeiko, 'Giant Josephson current through a single bound state in a superconducting tunnel junction', *Phys. Rev. B*, **53**, R6006 (1996). G. Wendin and V.S. Shumeiko, 'Josephson transport in complex mesoscopic structures', *Superlattices and Microstructures*, **20**, 569 (1996).

²⁸ C. Hu, 'Midgap Surface States as a Novel Signature for $d_{x^2-a^2}-d_{y^2-b^2}$ -Wave Superconductivity', *Phys. Rev. Lett.*, **72**, 1526 (1994).

²⁹ R.A. Riedel and P.F. Bagwell, 'Low-Temperature Josephson current peak in junctions with d-wave order parameters', *Physical Review B*, **57**, 6084 (1998).

³⁰ P.F. Bagwell, 'Critical Current of a One-Dimensional Superconductor', *Physical Review B*, **49**, 6841 (1994).

³¹ N. Argaman, 'Non-equilibrium Josephson-like effects in mesoscopic S-N-S junctions', preprint cond-mat/9709001.

³² A.M. Zagoskin, 'The Half-Periodic Josephson Effect in an s-Wave Superconductor - Normal Metal - d-Wave Superconductor Junction', *J. Phys.: Condens. Matter*, **9**, L419 (1997).